JOURNAL OF THE AMERICAN CHEMICAL SOCIETY

Subscriber access provided by Bethel University

Article

Assembly of Atomically Precise Silver Nanoclusters into Nanocluster-based Frameworks

Mohammad J. Alhilaly, Ren-Wu Huang, Rounak Naphade, Badriah Alamer,
Mohamed Nejib Hedhili, Abdul-Hamid Emwas, Partha Maity, Jun Yin, Aleksander
Shkurenko, Omar F. Mohammed, Mohamed Eddaoudi, and Osman M. Bakr

J. Am. Chem. Soc., **Just Accepted Manuscript** • DOI: 10.1021/jacs.9b02486 • Publication Date (Web): 28 May 2019

Downloaded from http://pubs.acs.org on May 28, 2019

Just Accepted

“Just Accepted” manuscripts have been peer-reviewed and accepted for publication. They are posted online prior to technical editing, formatting for publication and author proofing. The American Chemical Society provides “Just Accepted” as a service to the research community to expedite the dissemination of scientific material as soon as possible after acceptance. “Just Accepted” manuscripts appear in full in PDF format accompanied by an HTML abstract. “Just Accepted” manuscripts have been fully peer reviewed, but should not be considered the official version of record. They are citable by the Digital Object Identifier (DOI®). “Just Accepted” is an optional service offered to authors. Therefore, the “Just Accepted” Web site may not include all articles that will be published in the journal. After a manuscript is technically edited and formatted, it will be removed from the “Just Accepted” Web site and published as an ASAP article. Note that technical editing may introduce minor changes to the manuscript text and/or graphics which could affect content, and all legal disclaimers and ethical guidelines that apply to the journal pertain. ACS cannot be held responsible for errors or consequences arising from the use of information contained in these “Just Accepted” manuscripts.

is published by the American Chemical Society. 1155 Sixteenth Street N.W.,
Washington, DC 20036

Published by American Chemical Society. Copyright © American Chemical Society.
However, no copyright claim is made to original U.S. Government works, or works
produced by employees of any Commonwealth realm Crown government in the course
of their duties.

Assembly of Atomically Precise Silver Nanoclusters into Nanocluster-based Frameworks

Mohammad J. Alhilaly,[†,||,⊥] Ren-Wu Huang,[†,||] Rounak Naphade,[†,||] Badriah Alamer,[†,||] Mohamed Nejib Hedhili,[‡] Abdul-Hamid Emwas,[‡] Partha Maity,[†,||] Jun Yin,[†] Aleksander Shkurenko,[§] Omar F. Mohammed,[†] Mohamed Eddaoudi,[§] and Osman M. Bakr*[,†,||]

[†]Division of Physical Sciences and Engineering, King Abdullah University of Science and Technology (KAUST), Thuwal 23955-6900, Saudi Arabia

[||]KAUST Catalysis Center (KCC), Division of Physical Sciences and Engineering, King Abdullah University of Science and Technology (KAUST), Thuwal 23955-6900, Saudi Arabia

[‡]Core Labs, King Abdullah University of Science and Technology (KAUST), Thuwal 23955-6900, Saudi Arabia

[§]Functional Materials Design, Discovery and Development Research Group (FMD^3), Advanced Membranes and Porous Materials Center, King Abdullah University of Science and Technology (KAUST), Thuwal 23955-6900, Saudi Arabia

[⊥]Department of Physics, College of Sciences, Imam Mohammad Ibn Saud Islamic University (IMSIU), Riyadh, 11623, Saudi Arabia

---

ABSTRACT: Here, we demonstrate an approach for synthesizing and structurally characterizing three atomically precise anion-templated silver thiolate nanoclusters, two of which form one- and two-dimensional structural frameworks composed of bipyridine-linked nanocluster nodes (referred to as nanocluster-based frameworks, NCFs). We describe the critical role of the chloride (Cl^-) template in controlling the nanocluster's nuclearity with atomic precision; and the effect of a single Ag atom difference in the nanocluster's size in controlling the NCF dimensionality, modulating the optical properties, and improving the thermal stability. With atomically precise assembly and size control, nanoclusters could be widely adopted as building blocks for the construction of tunable cluster-based framework materials.

INTRODUCTION

One primary aim of nanotechnology is the bottom-up programmed assembly of materials from nano-sized building blocks with molecular precision and control. Unfortunately, most nanoparticles are atomically inhomogeneous, precluding their use as building blocks for such assembly. Atomically precise nanoparticles, also known as nanoclusters (NCs), are thus highly prized in the nanochemist's toolkit, as they make nanoparticles amenable to supramolecular assembly, property control, and materials interrogation (e.g., periodic structures amenable to single-crystal structure determination). Researchers have made tremendous strides in synthesizing metal and metal chalcogenide NCs with unique structures and distinct physicochemical properties;[1-5] for example, an impressive level of control over the size and surface ligand chemistry of such NCs has been achieved. However, relatively little progress has been made in developing and understanding the supramolecular chemistry associated with the assembly of NCs into crystalline solids. In fact, NCs reported to date typically crystallize into relatively trivial close-packed structures that lack diversity. The ability to control the NCs' coordination number affords the access to distinct secondary building units (SBUs) with assorted geometries and connectivity, defined by the arrangement of points of extensions on the NCs, and the prospective to construct periodic extended solids with fine-tuned porosity, reactivity, and conductivity, as well as optical and mechanical properties.[6-12]

Silver NCs stabilized with ligands (such as thiolate, alkynyl, or phosphine)[13-27] are ideal candidates for developing chemical approaches to the controlled self-assembly of solids. The size, composition, and surface chemistry of such NCs are reasonably well understood; however, there are enormous benefits to be gained from controlling the self-assembly modes of these NCs, stemming from their prospective applications in catalysis,[28-30] fluorescence sensing,[31] and bioimaging,[32] as well as anti-microbials[33]. The assembly of NCs into atomically precise NC-based frameworks would combine advantages from both NCs and metal-organic frameworks (MOFs), including: providing high nuclearlity cluster nodes, high structure tunability, highly connected frameworks with more structural complexity, large channels, and more robustness. These potential advantages are attractive for a wide range of potential applications including sensing, catalysis, and gas separation.[6, 34] Recently, Ag thiolate NCs, such as Ag_{10}, Ag_{12}, and Ag_{14},[34-36] have been shown to assemble into one-, two-, and three-dimensional frameworks in which the NCs form nodes connected by pyridyl-type organic linkers. In addition, several assembled structures of anion-templated Ag thiolate nanoclusters networked by short inorganic anions have also been reported.[37-38] The solvents used have also been found to play a critical role in the assemblies' morphology.[39] Despite advances in the synthesis of Ag-cluster-based MOFs in terms of boosting stability and enhancing optical properties, it remains challenging to produce atomically precise cluster-based frameworks (which is also referred to here as nanocluster-based frameworks, NCFs) with different dimensionalities. Indeed, studies on controlling cluster size in assembled networks with atomic precision or on the significant roles played by size and anion templates[40] – which are believed to affect the dimensionality and resulting properties – have yet to be reported.

In this work, we present a strategy for extending the size and dimensional control over Ag(I) thiolate NCs. In particular, we report three new crystal structures: a single Ag nanocluster (**0-D NC**) and two Ag nanocluster-based frameworks (**1-D NCF** and **2-D NCF**). Our approach relies on Cl^- as a template for NC growth in conjunction with a suitable organic linker, 4,4'-bipyridine (bpy), in the case of **1-D NCF** and **2-D NCF**. More specifically, when no organic linker (no bpy) is used, a Ag_{16} cluster is attained, which crystallizes as a discrete zero-dimensional structure (**0-D NC**). When bpy is added, depending on the ratio of the ligands (mainly the bpy linker) to the Ag thiolate complex, we found that two distinct clusters form: Ag_{15} and Ag_{14}, each adopting a MOF-like structure with specific dimensionality, i.e., **1-D NCF** and **2-D NCF**, respectively. The three cluster units in **0-D NC**, **1-D NCF**, and **2-D NCF** share notable similarities; in particular, the units possess a similar geometrical structure, in which the skeletons of cluster cores can be considered complete or incomplete square gyrobicupolas (Figure 1) and the protecting ligand shell of each cluster core contains a combination of the thiolate (^{t}BuS$^-$) and trifluoroacetate (CF_3COO^-) ligands, as well as coordinated solvent molecules. As the ratio of the ligands to the Ag thiolate complex increases (in the presence of bpy linker), clusters begin to distort more to accommodate structures of higher connectivity (and, thus, confined spacing). These distortions lead to a sequential loss of a single surface Ag atom as the NC adopts one- and two-dimensional assembled networks of Ag_{15} and Ag_{14} (**1-D NCF** and **2-D NCF**), respectively. Each of all these three structures (one silver NC and two cluster-based assembled networks) exhibits qualitatively distinct characteristics in photoluminescence (PL) and thermal stability. Specifically, higher-dimensional structures show enhanced PL and higher thermal stability.

Our approach represents a new method for controlling the nuclearity and dimensionality of self-assembled NCs, leading to novel atomically precise cluster-based MOF-like assembled materials, and at the same time modulating their optical properties. With improved control and understanding of the structures' self-assembly and size, we anticipate that metal NCs will provide a myriad of modular building blocks, with assorted shapes and connectivities, for the practice of reticular chemistry.

RESULTS AND DISCUSSION

Synthesis and characterization of 0-D NC, 1-D NCF and 2-D NCF. As illustrated in **Scheme 1**, a zero-dimensional Ag NC (**0-D NC**) and two Ag NC-based frameworks (**1-D NCF** and **2-D NCF**) were synthesized by a chemical reaction of the precursors using a one-pot approach. The chemical reaction initially occurred between the premade $[Ag\text{-}S^tBu]_n$ complex with silver trifluoroacetate in CH_3CN solvent to produce a homogeneous mixture under stirring. Then, a soluble dimethylformamide (DMF) solution of tetraphenylphosphonium chloride (PPh_4Cl) was added to form the Ag NCs. It is noted that the DMF solvent plays a critical role in facilitating the templating effect of Cl^-. To facilitate the assembly of the Ag clusters into one- and two-dimensional networks (**1-D NCF** and **2-D NCF**, respectively), bpy was added to the reaction mixture and utilized as an organic linker. By applying specific ratios of the precursors (see the experimental section for the synthesis details), rod-like green-emitting crystals of **2-D NCF** were obtained in high yield. By increasing the ratio of the independent ligands (bpy and $AgCF_3COO$ precursors) to the Ag thiolate complex, we found that the crystallization system tended to grow predominantly large **1-D NCF** crystals and small **2-D NCF** crystals (as a co-product). After the crystallization of the resulting clear solutions of the filtrates by slow evaporation at room temperature, high-quality single crystals suitable for single-crystal X-ray diffraction (SCXRD) were obtained after 7-12 days. The crystal structures of **0-D NC**, **1-D NCF**, and **2-D NCF** were studied by SCXRD, and the phase purities were evaluated by PXRD. Furthermore, the optical properties and thermal stability of the structures were studied. The synthesis and crystallization details of all three products can be found in the experimental section.

Scheme 1. Synthesis of Ag NC and NC-based frameworks

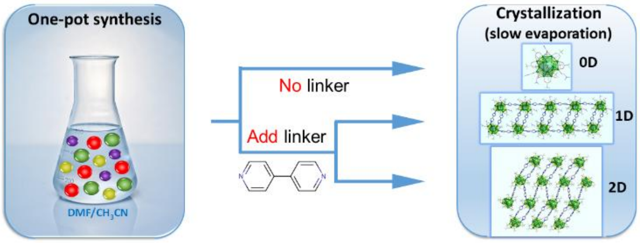

Single-crystal structures of 0-D NC, 1-D NCF, and 2-D NCF. $[Ag_{16}Cl(S^tBu)_8(CF_3COO)_7(DMF)_4(H_2O)]\cdot1.5(DMF)$ (**0-D NC**). First, a crystal of **0-D NC** was evaluated by SCXRD. Analysis of the crystallographic data showed that **0-D NC** crystallizes in the monoclinic space group *C*2/*c* (Table S1). The structure of **0-D NC** is essentially a silver cluster with a Ag_{16} skeleton welded by argentophilic interactions; the Ag_{16} cluster is templated by one enclosed Cl^- at the center and forms a distorted square gyrobicupola (29th Johnson solid, J29),[41] which is a polyhedron with eight triangular and ten distorted square faces (Figure 1A). Among these polygons, each square face is capped by a $^tBuS^-$ ligand (except for the top and bottom faces) with a consistent μ_4-η^1:η^1:η^1:η^1-ligation mode to link four silver ions with Ag–S distances in the range of 2.368(2)–2.598(2) Å (Figures 2, top). The skeleton is also protected by seven CF_3COO^- auxiliary ligands (Figure S1). Five of those ligands bind to the equatorial plane (octagonal Ag_8) of the polyhedron through Ag–O bonds adopting the μ_2-η^1:η^1 mode (Ag–O: 2.19(3)–2.474(6) Å). The remaining two CF_3COO^- ligands cap the upper (μ_3-η^1:η^2 mode) and lower (μ_2-η^1:η^1 mode) square faces with Ag–O bonds in the ranges of 2.40(1)–2.68(2) and 2.483(8)–2.69(3) Å, respectively. The protecting ligand shell also contains four DMF molecules and one H_2O molecule coordinated in the equatorial plane (Figure S4, left). In addition, the Ag_{16} cluster structure includes one and a half molecules of the co-crystallized DMF solvents (Figure S5, left). Interestingly, within the skeleton, the distances between the central Cl^- and peripheral Ag atoms, in the range of 2.789(2)–3.608(2) Å, are much longer than those of conventional Ag–Cl bonds (approximately 2.6 Å). A similar situation has been observed for alkynyl-protected silver clusters.[14, 42-43] The anion templating effect of Cl^- is quite important for the assembly of the skeleton structure. It is worth noting that the argentophilic interactions also play a crucial role in the stabilization of the silver cluster skeleton. The observed Ag···Ag distances range from 2.919(2) to 3.286(2) Å, which are shorter than twice the van der Waals radius of silver (3.44 Å), indicating significant argentophilic interactions.

$[Ag_{15}Cl(S^tBu)_8(CF_3COO)_{5.67}(NO_3)_{0.33}(bpy)_2(DMF)_2]\cdot4.3(DMF)\cdot H_2O$ (**1-D NCF**). Crystallographic data analysis of **1-D NCF** showed that its crystal structure contains a Ag_{15} cluster also templated by Cl^- and belongs to the triclinic space group *P*–1 (Table S2). The skeleton of the Ag_{15} cluster core is composed of an incomplete distorted square gyrobicupola through the argentophilic interactions, with Ag···Ag bond distances in the range of 2.912(1)–3.381(1) Å, due to one missing Ag atom; the polyhedron contains six triangular and eight square faces (Figure 1B). The skeleton is protected by eight $^tBuS^-$ ligands that adopt two types of coordination modes—six adopt the μ_4-η^1:η^1:η^1:η^1-ligation mode and two adopt the μ_3-η^1:η^1:η^1-ligation mode—where the Ag–S distances are in the range of 2.338(3)–2.576(2) Å. The structure also features a clear distortion, as shown in Figure 2 (middle). In contrast to the four coordinated DMF molecules in the Ag_{16} NC (**0-D NC**), only two coordinated DMF molecules were observed in the Ag_{15} cluster of **1-D NCF**. Likewise in the previous structure, the Ag_{15} is co-protected by CF_3COO^- auxiliary ligands: four of them are coordinated in the equatorial plane in the μ_2-η^1:η^1 mode with Ag–O distances in the range of 2.299(6)–3.054(8) Å; the ligands are found in the upper (μ_3-η^1:η^2 mode) and lower axial positions (μ_2-η^1:η^1 mode) with Ag–O distances in the range of 2.450(8)–2.709(7) and 2.399(8)–2.60(2) Å, respectively. The number of CF_3COO^- auxiliary ligands was also observed to decrease proportionally as one Ag atom was lost to balance the charge. Interestingly, this compound is found to contain the substitutional disorder of one auxiliary ligand bonded to the equatorial Ag atom, with an occupancy of 0.67 for CF_3COO^- and 0.33 for NO_3^-. The unanticipated NO_3^- may be derived from the residual silver nitrate in the $[Ag\text{-}S^tBu]_n$ complex precursor (Figure S4, middle). Finally, each Ag_{15} cluster is connected to three adjacent such clusters through four bpy linkers to form an infinite one-dimensional (1D) ladder-like structure. In this structure, dual-cluster units, each consisting of two clusters and two juxtaposed bpy monomer pillars, are further combined by single-bpy bridges along the *b*-axis only. The dual-cluster unit is inclined relative to the single-bpy bridges at an acute angle of approximately 70° (Figure 3B).

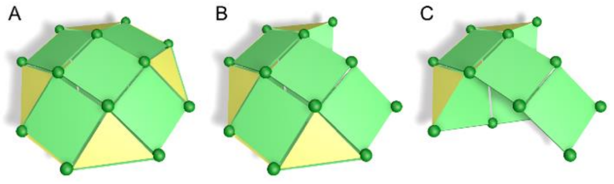

Figure 1. Geometrical structures of the cores of **0-D NC** (A), **1-D NCF** (B), and **2-D NCF** (C).

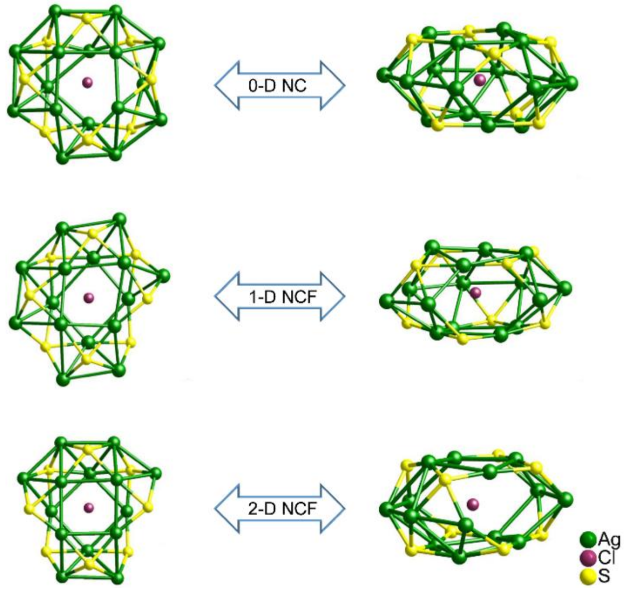

Figure 2. Top view vs. side view comparison between core structures of **0-D NC** (top), **1-D NCF** (middle), and **2-D NCF** (bottom).

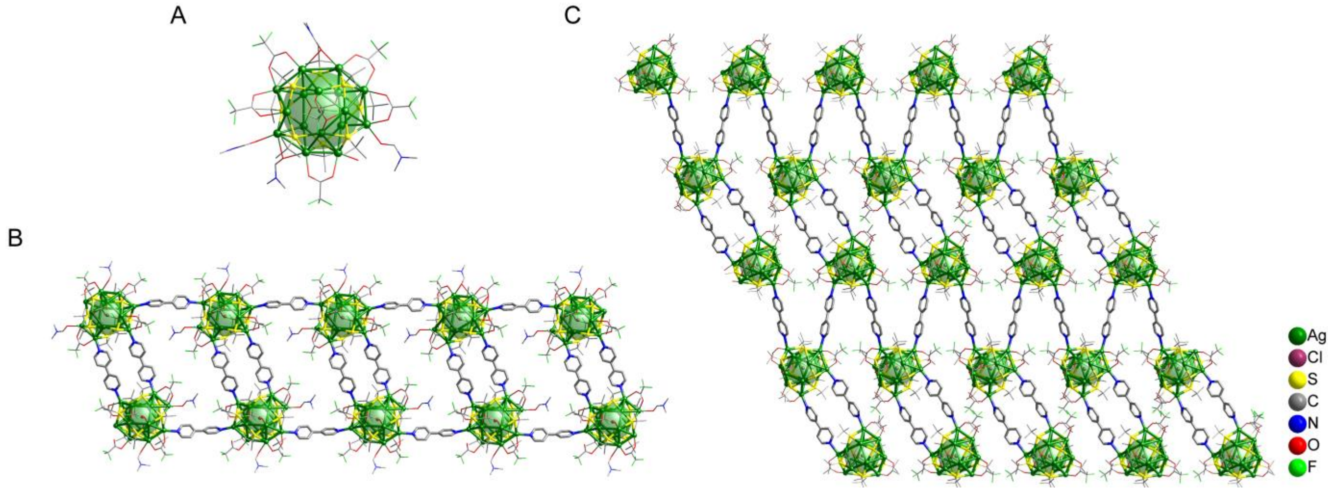

Figure 3. Crystal structures of **0-D NC** (A), **1-D NCF** (B), and **2-D NCF** (C). Free (co-crystallized) DMF molecules are not shown. The green semi-transparent spheres in the silver clusters are shown purely as a guide. Hydrogens have been omitted for clarity.

[Ag$_{14}$Cl(S^{t}Bu)$_8$(CF$_3$COO)$_5$(bpy)$_2$(DMF)]·2(DMF) (**2-D NCF**). Crystallizing in the triclinic space group *P*–1 (Table S3), **2-D NCF** is formed by a Ag$_{14}$ cluster that, similarly to **0-D NC** and **1-D NCF**, is also assembled by a templating chloride. The Ag$_{14}$ skeleton is considered an incomplete square gyrobicupola and assembles into a two-dimensional structure of networked Ag$_{14}$ cluster nodes (Figures 2, bottom and 3C). Because two of the original 16 Ag atoms are missing, the Ag$_{14}$ skeleton features only four triangular and six square faces constructed via sparse argentophilic interactions (Ag···Ag distances in the range of 2.890(1)–3.4072(8) Å) and is co-protected by eight ^{t}BuS$^-$ ligands, five CF$_3$COO$^-$ auxiliary ligands, and only one coordinated DMF molecule (Figures S4 and S5, right). We found that the eight ^{t}BuS$^-$ ligands adopt two types of coordination modes: four adopt the μ_4-η^1:η^1:η^1:η^1-ligation mode, and the other four adopt the μ_3-η^1:η^1:η^1-ligation mode. The range of Ag–S distances is 2.34(2)–2.558(2) Å. The five CF$_3$COO$^-$ ligands can also be classified into two groups. Similarly to the structures described above, the equatorial and one axial CF$_3$COO$^-$ ligands are coordinated in the μ_2-η^1:η^1 mode, while the second axial ligand is coordinated in the μ_3-η^1:η^2-ligation mode. The Ag–O distances range from 2.288(6) to 2.93(1) Å. Furthermore, each Ag$_{14}$ cluster coordinates to four bpy linkers. Consequently, two clusters and two parallel bpy linkers are employed to construct a dual-cluster unit similar to that in **1-D NCF**. Each dual-cluster unit is further connected to four others in the upper and lower rows by single-bpy_bridges to form a 2D framework, in which the Ag$_{14}$ clusters are regarded as the nodes of the 2D framework (Figure 3C). In other words, two of the Ag$_{14}$ clusters are directed towards the same neighbor, forming a "dual-cluster unit", as observed in **1-D NCF**. From a topological point of view, the two linkers there act as one edge (Figure S7B). Since the next two bpy spacers are directed toward different Ag$_{14}$ clusters, two-dimensional framework formation is observed, where each Ag$_{14}$ cluster is a 3-c node and the entire two-dimensional framework is a 3-c, 2-periodic edge transitive net called **hcb** (Figure S7C). Finally, the adjacent 2D layers are further extended into a 3D supramolecular structure via weak hydrogen bonds between the terminal *t*-butyl and trifluoromethyl groups on the surface of the adjacent layers (Figure S8). The layers are slightly offset with respect to each other; thus, two types of channels in the **2-D NCF** crystal structure are observed: the channels oriented along the direction [1 -1 0] are parallel to the layers, whereas the channels oriented along the crystallographic *a*-axis penetrates them. Two non-coordinated DMF molecules were localized in the channels, and the contribution of the significantly delocalized electron density was excluded from the refinement by the PLATON SQUEEZE[44] procedure.

Optical absorption and photoluminescence properties of 0-D NC, 1-D NCF, and 2-D NCF. We measured the optical absorption spectra of **0-D NC** in solution and solid-state (Figure S9). Crystals of **0-D NC** display a clear absorption band in the UV region (~200-350 nm), as shown in Figure S9(top). Crystals of **1-D NCF** and **2-D NCF** also exhibit absorption bands in the UV region, but both show an additional shoulder peak at ~420 nm (Figures S10 and S11). This shoulder is only observed for **1-D NCF** and **2-D NCF**, possibly due to residual solvent (DMF molecules) within the networked cluster nodes, as the shoulder peak becomes less intense (or nearly disappears) with more efficient drying of the crystals.

Crystals of **2-D NCF** exhibit clear green emission at ~530 nm with excitation at 365 nm at room temperature (~298 K) under ambient conditions (Figure S12). In contrast, the emissions of **0-D NC** and **1-D NCF** at room temperature are not visually detectable; indeed, we could not observe any steady-state PL under UV light (365 nm). Nevertheless, we were able to detect weak emissions of **0-D NC** and **1-D NCF** at lower temperatures using temperature-dependent photoluminescence (TDPL). The maximum emission wavelen-

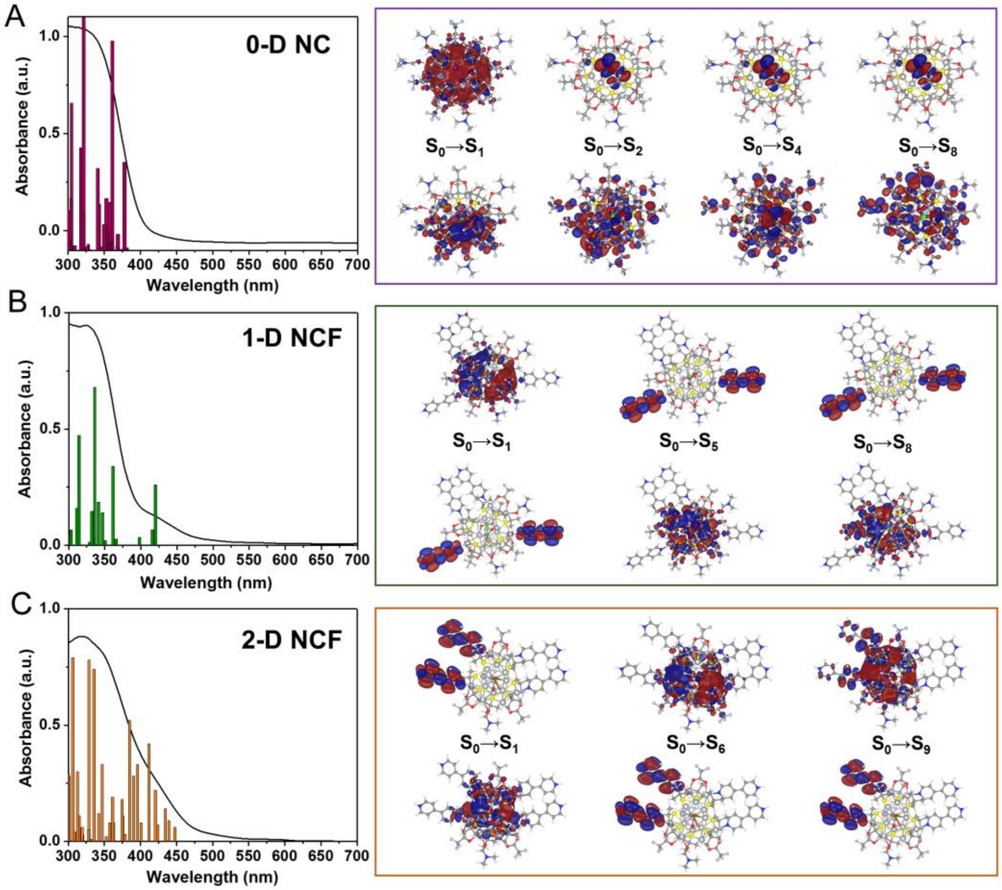

Figure 4. Experimental absorption spectra (solid black lines) with calculated optical transition wavelengths and oscillator strengths (vertical lines) using TDDFT method and the dominant natural transition orbital (NTO) hole and particle pairs (isovalue = 0.02 $e\cdot Å^{-3}$) for the main singlet excited states of (A) **0-D NC**, (B) **1-D NCF**, and (C) **2-D NCF**.

gth of the TDPL of **0-D NC** occurs at ~535 nm, with no notable spectral shift with varying temperature; the spectrum also shows a shoulder peak at ~430 nm (Figure S13). We observed a clear, systematic decrease in the **0-D NC** emission intensity with increasing temperature. **1-D NCF** crystals display similar emission spectra as **0-D NC** crystals, exhibiting the same emission at ~535 nm, with no clear shift with changing temperature, and the shoulder peak (~430 nm) is also observed (Figure S14). However, **0-D NC** shows sensitivity to UV light; specifically, a change in color is observed as a result of degradation induced by UV light (at excitation wavelength 365 nm). We also examined the TDPL of **2-D NCF** crystals, which exhibit distinctly stronger emission, as shown in Figure S15. A systematic spectral red shift was observed with an increase in temperature from 77 K to room temperature, with the emission wavelength varying from ~511 to 540 nm under excitation at 325 nm. Furthermore, given the appreciable PL signal of **2-D NCF** crystals, a PL lifetime of 0.32 μs was measurable (excitation at 372 nm), which may originate from the radiative recombination of the excited triplet state (Figure S16).[34-35] The results of the optical investigation of the three species clearly show that **2-D NCF**, which possesses the highest dimensionality among the three structures, displays enhanced PL properties. Such PL enhancement could be attributed to the linker-to-cluster charge-transfer state as explained from DFT calculations (*vide infra*).

DFT calculations. We performed time-dependent density functional theory (TDDFT) calculations to study the major optical transitions of **0-D NC**, **1-D NCF** and **2-D NCF**. Overall, as shown in Figure 4, our calculated optical transition wavelengths and oscillator strengths are in reasonably good match with the experimental absorption spectra. For **0-D NC**, most absorption peaks with a large oscillator strength (S_1, S_2, S_4, and S_8) can be assigned to the electronic transitions of a "hole" delocalized in the Ag_{16} cluster to the "particle" localized partially in the cluster core using natural transition orbital (NTO) analysis. However, for both **1-D NCF** and **2-D NCF**, the excitation induced by light irradiation can effectively shift the electronic distribution from the hole/particle localized in organic linkers to the delocalized particle/hole in the cluster core. In contrast to the cluster-to-linker feature of the $S_1 \rightarrow S_0$ transition in **1-D NCF**, the enhanced PL intensity observed for **2-D NCF**

could be attributed to linker-to-cluster charge-transfer excitation.

Other characterizations. PXRD measurements confirmed the crystallinity and phase purity of the three structures based on the agreement between the experimental and simulated spectra (Figure S17). Thermogravimetric analysis (TGA) measurements were conducted to monitor the thermal stability of the structures. As shown in Figure S18, the main weight loss for **0-D NC** occurs at ~124°C. This loss corresponds to the complete decomposition of the building blocks of Ag_{16} clusters. The TGA of **1-D NCF** showed a large drop corresponding to the main loss of mass at ~150°C. We found that less distinct weight loss occurs at low temperatures for better air-dried samples; therefore, the initial loss is due to residual DMF solvent. The main loss most likely corresponds to the complete decomposition of the Ag cluster-building units. In **2-D NCF**, similar TGA behavior was observed, but the main loss occurred at ~160°C, which indicates that the structure is more robust. Thus, the TGA results indicate a clear improvement in thermal stability and robustness with increasing dimensionality from **0-D NC** to **2-D NCF**. Additionally, we evaluated the thermal stability of NCFs through monitoring the PL retention and recovery (from 0-100°C). The data show that **2-D NCF** have retained most of its PL, indicating that **2-D NCF** is more thermally stable than **1-D NCF** (Figure S19).

Fourier transform infrared (FTIR) spectroscopy was performed on powder samples. The broad peak around 3400 cm^{-1} in the **0-D NC** spectrum is assigned to the OH stretching vibration of water molecule (which confirms the coordinated H_2O in **0-D NC** only). However, the peak between 2800 cm^{-1} and 3000 cm^{-1} is observed in all structures—**0-D NC**, **1-D NCF**, and **2-D NCF**—and corresponds to the terminal C–H of *tert*-butyl functional group in the thiolate ligand. The obtained sharp peak at ~1640 cm^{-1} is observed in all the three structures which is assigned to the C=O stretching vibration of the DMF molecules in the crystal structures. In addition, an extra shoulder peak at ~1595 cm^{-1} is only observed in **1-D NCF** and **2-D NCF**, which can be assigned to the C–N stretching vibration from the bpy linker (Figure S20).

Furthermore, X-ray photoelectron spectroscopy (XPS) was performed to characterize the chemical composition of the surface of a **2-D NCF** crystal sample and to determine the oxidation state of chlorine. The survey spectrum of the **2-D NCF** crystal sample shows that Ag, S, F, Cl, O and C were detected (Figure S21). The high-resolution XPS spectrum of the Cl 2p core level was obtained from the **2-D NCF** crystal sample. The Cl 2p region shows one doublet positioned at 198.2 eV and 199.8 eV corresponding to the Cl $2p_{3/2}$ and Cl $2p_{1/2}$ spin–orbit split components, respectively (Figure S22, top). For comparison, the high-resolution XPS spectrum of the Cl 2p core level was obtained from the PPh_4Cl precursor. The Cl 2p region shows one doublet situated at 196.2 eV and 197.8 eV corresponding to the Cl $2p_{3/2}$ and Cl $2p_{1/2}$ spin–orbit split components, respectively (Figure S22, bottom). These binding energies correspond to the ionic form of free chlorine (Cl^-) in PPh_4Cl.[45] The shift in the Cl $2p_{3/2}$ component from low binding energy at 196.2 eV for the PPh_4Cl precursor to high binding energy at 198.2 eV for the **2-D NCF** crystal sample indicates that Cl^- interacts strongly with the silver skeleton around it in the **2-D NCF** crystal compared with the free Cl^- ions in PPh_4Cl.

Consistent with the SCXRD results, solid-state ^{13}C nuclear magnetic resonance (NMR) spectroscopy was also performed for the crystals of **0-D NC**, **1-D NCF**, and **2-D NCF**. Different DMF-CH_3 peaks were observed at 31.16 and 32.22 ppm and at 45.99 and 47.91 ppm, which were associated with the bonded-DMF and free-DMF environments, respectively. Moreover, the carbonyl C peak was observed to split into two peaks at 161.74 ppm due to free DMF molecules and formed one extra peak at 165.34 due to coordinated DMF. Due to F-C coupling, the CF_3 peak split into different lines at 114.68, 116.59, 118.71, and 122.25 ppm, while a peak attributed to COOAg was observed at 159.82 ppm. The strong peak observed at 36.88 ppm was assigned to methyl groups of $^tBuS^-$, and a quaternary carbon peak appeared at 51.09 ppm. A comparison of the **0-D NC** spectrum with the **1-D NCF** and **2-D NCF** spectra shows extra peaks in the aromatic region (122.31, 146.26, and 151.56 ppm), which can be assigned to the aromatic peaks of the bpy linker (Figure S23).[46]

In addition, to further corroborate the molecular formula and purity of **0-D NC**, electrospray ionization mass spectrometry (ESI-MS) measurements were performed on the crystals of **0-D NC** dissolved in CH_3CN solvent (as shown in Figure S24). The assignments of the mass peaks demonstrate a clear match between isotopic patterns of the experimental and simulated mass spectra (Figure S24, a, b, and c). The deduced molecular formula from ESI-MS is in good agreement with the crystal structure obtained by SCXRD.

CONCLUSION

To conclude, we report three novel structures of atomically precise chloride-templated Ag(I) thiolate nanoclusters and nanocluster-based frameworks (**0-D NC**, **1-D NCF**, and **2-D NCF**). By employing four main reaction levers (Cl^- anion template, DMF solvent, bpy linker, and reactant/precursor ratio), we successfully achieved the controlled assembly of a well-defined zero-dimensional Ag_{16} cluster (**0-D NC**) and two cluster-based assembled networks, Ag_{15} (**1-D NCF**) and Ag_{14} (**2-D NCF**) with atomic-level control over cluster size and dimensionality. The change in dimensionality offers a distinct way to tune the optical and PL properties (as well as to improve the thermal stability) of cluster-based frameworks. This study paves the way for synthesizing new functional nanomaterials of cluster-based MOFs with full atomic precision and utilizing their tunable properties for a wide range of potential applications.

EXPERIMENTAL SECTION

Materials. All the following chemicals and solvents were purchased and used without further purification: silver nitrate ($AgNO_3$, 99%, Aldrich), silver trifluoroacetate ($AgCF_3COO$, 98%, Aldrich), tetraphenylphosphonium chloride (PPh_4Cl, 98%, Aldrich), tert-butyl mercaptan (99%, Aldrich), trimethylamine (99%, pure, ACROS), 4,4'-bipyridine (bpy, 98%, Aldrich), dichloromethane (DCM, HPLC grade, VWR), methanol (MeOH, HPLC grade, VWR), *N*,*N*-dimethylformamide (DMF, HPLC grade, Aldrich), and acetonitrile (CH_3CN, HPLC grade, Aldrich).

Synthesis of $[Ag\text{-}S^tBu]_n$ complex. The complex was prepared according to a previously reported method[47] but with some modifications. First, $AgNO_3$ (3 mmol) was completely dissolved in 20 mL of MeOH by sonication. In another vial, tert-butyl mercaptan (3 mmol) was dissolved in 10 mL of DCM and directly added to the methanolic solution of $AgNO_3$. Then, triethylamine (~1 mmol) was added quickly to the reaction mixture under stirring. The reaction was continued at room temperature (RT) in the dark overnight. The next day, the sample was centrifuged at 8000 rpm for 5 min; the white precipitate of the complex was washed at least 5 times with MeOH and then stored under vacuum for further use.

Synthesis and crystallization of 0-D NC. In a glass vial, ~0.3 mmol of $[Ag\text{-}S^tBu]_n$ and ~0.2 mmol of $AgCF_3COO$ were mixed in 5 mL of CH_3CN and stirred for ~5 min. Then, 4 mL of a soluble DMF solution of PPh_4Cl (~0.04 mmol) was immediately added to the reaction mixture with stirring, and the reaction was continued for ~2 h at RT. After filtration, the filtrate was allowed to evaporate slowly at room temperature in the dark under ambient conditions. After 9-12 days, colorless crystals were obtained. Average yield of **0-D NC**: 47.8 % (based on Ag).

Synthesis and crystallization of 1-D NCF and 2-D NCF mixture. In a glass vial, ~0.34 mmol of $[Ag\text{-}S^tBu]_n$, ~0.26 mmol of $AgCF_3COO$ and ~0.38 mmol bpy were mixed together in 5 mL of CH_3CN with stirring for ~5 min. Then, 4 mL of a soluble DMF solution of PPh_4Cl (~0.06 mmol) was added to the reaction mixture, and the reaction was continued under stirring for ~2 h at room temperature. The filtrate was then allowed to evaporate slowly at RT in the dark under ambient conditions. Large reddish crystals of **1-D NCF** in addition to small **2-D NCF** crystals were obtained after one week of crystallization. Average yield of **1-D NCF**: 35.6 % (based on Ag).

Synthesis and crystallization of 2-D NCF. In a glass vial, 0.3 mmol of $[Ag\text{-}S^tBu]_n$, 0.2 mmol of $AgCF_3COO$ and 0.3 mmol of bpy were mixed together in 5 mL of CH_3CN with stirring for ~5 min. Then, 4 mL of a soluble DMF solution of PPh_4Cl (0.04 mmol) was added to the reaction mixture, and the reaction was continued under stirring for ~2 h at room temperature. The filtrate was then allowed to evaporate slowly at RT in the dark under ambient conditions. Colorless rod-like crystals were obtained after one week of crystallization. Average yield of **2-D NCF**: 55.6 % (based on Ag).

ASSOCIATED CONTENT

Supporting Information. Instrumentation, UV–vis, steady-state PL, PL lifetime, PXRD, XPS, TGA, FTIR, ^{13}C NMR, ESI-MS, and analyses of crystal structures of **0-D NC**, **1-D NCF**, and **2-D NCF**. This material is available free of charge via the Internet at http://pubs.acs.org.

AUTHOR INFORMATION

Corresponding Author

*osman.bakr@kaust.edu.sa

Notes

The authors declare no competing financial interests.

ACKNOWLEDGMENT

The authors would like to deeply thank the following people for their help and dedication at various stages of this project: Ayalew Assen, Karim Adil, and Osama Shekhah. The financial support for this work was provided by KAUST.

REFERENCES

(1) Jin, R.; Zeng, C.; Zhou, M.; Chen, Y. Atomically precise colloidal metal nanoclusters and nanoparticles: fundamentals and opportunities. *Chem. Rev.* **2016,** *116* (18), 10346–10413.
(2) Chakraborty, I.; Pradeep, T. Atomically precise clusters of noble metals: emerging link between atoms and nanoparticles. *Chem. Rev.* **2017,** *117* (12), 8208-8271.
(3) Kurashige, W.; Niihori, Y.; Sharma, S.; Negishi, Y. Precise synthesis, functionalization and application of thiolate-protected gold clusters. *Coord. Chem. Rev.* **2016,** *320-321*, 238-250.
(4) Fuhr, O.; Dehnen, S.; Fenske, D. Chalcogenide clusters of copper and silver from silylated chalcogenide sources. *Chem. Soc. Rev.* **2013,** *42* (4), 1871-1906.
(5) Jin, R.; Pei, Y.; Tsukuda, T. Controlling nanoparticles with atomic precision. *Acc. Chem. Res.* **2019,** 52 (1), 1-1.
(6) Kalmutzki, M. J.; Hanikel, N.; Yaghi, O. M. Secondary building units as the turning point in the development of the reticular chemistry of MOFs. *Sci. Adv.* **2018,** *4* (10), eaat9180.
(7) Guillerm, V.; Weseliński, Ł. J.; Belmabkhout, Y.; Cairns, A. J.; D'Elia, V.; Wojtas, Ł.; Adil, K.; Eddaoudi, M. Discovery and introduction of a (3,18)-connected net as an ideal blueprint for the design of metal–organic frameworks. *Nat. Chem.* **2014,** *6*, 673.
(8) Alezi, D.; Peedikakkal, A. M. P.; Weseliński, Ł. J.; Guillerm, V.; Belmabkhout, Y.; Cairns, A. J.; Chen, Z.; Wojtas, Ł.; Eddaoudi, M. Quest for highly connected metal–organic framework platforms: rare-earth polynuclear clusters versatility meets net topology needs. *J. Am. Chem. Soc.* **2015,** *137* (16), 5421-5430.
(9) Ji, Z.; Trickett, C.; Pei, X.; Yaghi, O. M. Linking Molybdenum–sulfur clusters for electrocatalytic hydrogen evolution. *J. Am. Chem. Soc.* **2018,** *140* (42), 13618-13622.
(10) Schoedel, A.; Yaghi, O. M. Reticular chemistry of metal–organic frameworks composed of copper and zinc metal oxide secondary building units as nodes. In *The Chemistry of Metal–Organic Frameworks* (ed. Kaskel, S.), Wiley-VCH Verlag GmbH & Co. KGaA, **2016,** 43-72.
(11) Eddaoudi, M.; Moler, D. B.; Li, H.; Chen, B.; Reineke, T. M.; O'Keeffe, M.; Yaghi, O. M. Modular Chemistry: Secondary Building units as a basis for the design of highly porous and robust metal–organic carboxylate frameworks. *Acc. Chem. Res.* **2001,** *34* (4), 319-330.

(12) Yaghi, O. M.; O'Keeffe, M.; Ockwig, N. W.; Chae, H. K.; Eddaoudi, M.; Kim, J. Reticular synthesis and the design of new materials. *Nature* **2003,** *423*, 705.

(13) Joshi, C. P.; Bootharaju, M. S.; Bakr, O. M. Tuning properties in silver clusters. *J. Phys. Chem. Lett.* **2015,** *6* (15), 3023-3035.

(14) Rais, D.; Yau, J.; Mingos, D. M. P.; Vilar, R.; White, A. J. P.; Williams, D. J. Anion-templated syntheses of rhombohedral silver–alkynyl cage compounds. *Angew. Chem. Int. Ed.* **2001,** *40* (18), 3464-3467.

(15) Liu, C.; Li, T.; Abroshan, H.; Li, Z.; Zhang, C.; Kim, H. J.; Li, G.; Jin, R. Chiral Ag23 nanocluster with open shell electronic structure and helical face-centered cubic framework. *Nat. Commun.* **2018,** *9* (1), 744.

(16) Joshi, C. P.; Bootharaju, M. S.; Alhilaly, M. J.; Bakr, O. M. [Ag25(SR)18]–: the "golden" silver nanoparticle. *J. Am. Chem. Soc.* **2015,** *137* (36), 11578-11581.

(17) AbdulHalim, L. G.; Bootharaju, M. S.; Tang, Q.; Del Gobbo, S.; AbdulHalim, R. G.; Eddaoudi, M.; Jiang, D.-e.; Bakr, O. M. Ag29(BDT)12(TPP)4: a tetravalent nanocluster. *J. Am. Chem. Soc.* **2015,** *137* (37), 11970-11975.

(18) Desireddy, A.; Conn, B. E.; Guo, J.; Yoon, B.; Barnett, R. N.; Monahan, B. M.; Kirschbaum, K.; Griffith, W. P.; Whetten, R. L.; Landman, U.; Bigioni, T. P. Ultrastable silver nanoparticles. *Nature* **2013,** *501* (7467), 399-402.

(19) Yang, H.; Wang, Y.; Huang, H.; Gell, L.; Lehtovaara, L.; Malola, S.; Häkkinen, H.; Zheng, N. All-thiol-stabilized Ag44 and Au12Ag32 nanoparticles with single-crystal structures. *Nat. Commun.* **2013,** *4*. 2422.

(20) Jin, S.; Wang, S.; Song, Y.; Zhou, M.; Zhong, J.; Zhang, J.; Xia, A.; Pei, Y.; Chen, M.; Li, P.; Zhu, M. Crystal structure and optical properties of the [Ag62S12(SBut)32]2+ nanocluster with a complete face-centered cubic kernel. *J. Am. Chem. Soc.* **2014,** *136* (44), 15559-15565.

(21) Wang, Z.; Su, H.-F.; Kurmoo, M.; Tung, C.-H.; Sun, D.; Zheng, L.-S. Trapping an octahedral Ag6 kernel in a seven-fold symmetric Ag56 nanowheel. *Nat. Commun.* **2018,** *9* (1), 2094.

(22) Alhilaly, M. J.; Bootharaju, M. S.; Joshi, C. P.; Besong, T. M.; Emwas, A.-H.; Juarez-Mosqueda, R.; Kaappa, S.; Malola, S.; Adil, K.; Shkurenko, A.; Häkkinen, H.; Eddaoudi, M.; Bakr, O. M. [Ag67(SPhMe2)32(PPh3)8]3+: synthesis, total structure, and optical properties of a large box-shaped silver nanocluster. *J. Am. Chem. Soc.* **2016,** *138* (44), 14727-14732.

(23) Chai, J.; Yang, S.; Lv, Y.; Chen, T.; Wang, S.; Yu, H.; Zhu, M. A unique pair: Ag40 and Ag46 nanoclusters with the same surface but different cores for structure–property correlation. *J. Am. Chem. Soc.***2018,** *140* (46), 15582-15585.

(24) Bodiuzzaman, M.; Ghosh, A.; Sugi, K. S.; Nag, A.; Khatun, E.; Varghese, B.; Paramasivam, G.; Antharjanam, S.; Natarajan, G.; Pradeep, T. Camouflaging structural diversity: co-crystallization of two different nanoparticles having different cores but the same shell. *Angew. Chem. Int. Ed.* **2019,** *58* (1), 189-194.

(25) Song, Y.; Lambright, K.; Zhou, M.; Kirschbaum, K.; Xiang, J.; Xia, A.; Zhu, M.; Jin, R. Large-scale synthesis, crystal structure, and optical properties of the Ag146Br2(SR)80 nanocluster. *ACS Nano* **2018,** *12* (9), 9318-9325.

(26) Yang, H.; Wang, Y.; Chen, X.; Zhao, X.; Gu, L.; Huang, H.; Yan, J.; Xu, C.; Li, G.; Wu, J.; Edwards, A. J.; Dittrich, B.; Tang, Z.; Wang, D.; Lehtovaara, L.; Häkkinen, H.; Zheng, N. Plasmonic twinned silver nanoparticles with molecular precision. *Nat. Commun.* **2016,** *7*, 12809.

(27) Li, S.; Du, X.-S.; Li, B.; Wang, J.-Y.; Li, G.-P.; Gao, G.-G.; Zang, S.-Q. Atom-precise modification of silver(i) thiolate cluster by shell ligand substitution: a new approach to generation of cluster functionality and chirality. *J. Am. Chem. Soc.* **2018,** *140* (2), 594-597.

(28) Zhao, S.; Jin, R.; Jin, R. Opportunities and challenges in CO2 Reduction by gold- and silver-based electrocatalysts: from bulk metals to nanoparticles and atomically precise nanoclusters. *ACS Energy Lett.* **2018,** *3* (2), 452-462.

(29) Yan, J.; Zhang, J.; Chen, X.; Malola, S.; Zhou, B.; Selenius, E.; Zhang, X.; Yuan, P.; Deng, G.; Liu, K.; Su, H.; Teo, B. K.; Häkkinen, H.; Zheng, L.; Zheng, N. Thiol-stabilized atomically precise, superatomic silver nanoparticles for catalysing cycloisomerization of alkynyl amines. *Natl. Sci. Rev.* **2018,** *5* (5), 694-702.

(30) Chang, Z.; Jing, X.; He, C.; Liu, X.; Duan, C. Silver clusters as robust nodes and π–activation sites for the construction of heterogeneous catalysts for the cycloaddition of propargylamines. *ACS Catal.* **2018,** *8* (2), 1384-1391.

(31) Zhang, J.; Cheng, F.; Li, J.; Zhu, J.-J.; Lu, Y. Fluorescent nanoprobes for sensing and imaging of metal ions: recent advances and future perspectives. *Nano Today* **2016,** *11* (3), 309-329.

(32) Song, X.-R.; Goswami, N.; Yang, H.-H.; Xie, J. Functionalization of metal nanoclusters for biomedical applications. *Analyst* **2016,** *141* (11), 3126-3140.

(33) Zheng, K.; Setyawati, M. I.; Leong, D. T.; Xie, J. Antimicrobial silver nanomaterials. *Coord. Chem. Rev.* **2018,** *357*, 1-17.

(34) Huang, R.-W.; Wei, Y.-S.; Dong, X.-Y.; Wu, X.-H.; Du, C.-X.; Zang, S.-Q.; Mak, T. C. W. Hypersensitive dual-function luminescence switching of a silver-chalcogenolate cluster-based metal–organic framework. *Nat. Chem.* **2017,** *9*, 689.

(35) Wang, Z.-Y.; Wang, M.-Q.; Li, Y.-L.; Luo, P.; Jia, T.-T.; Huang, R.-W.; Zang, S.-Q.; Mak, T. C. W. Atomically precise site-specific tailoring and directional assembly of superatomic silver nanoclusters. *J. Am. Chem. Soc.* **2018,** *140* (3), 1069-1076.

(36) Dong, X.-Y.; Huang, H.-L.; Wang, J.-Y.; Li, H.-Y.; Zang, S.-Q. A flexible fluorescent SCC-MOF for switchable molecule identification and temperature display. *Chem. Mater.* **2018,** *30* (6), 2160-2167.

(37) Wang, Z.; Li, X.-Y.; Liu, L.-W.; Yu, S.-Q.; Feng, Z.-Y.; Tung, C.-H.; Sun, D. Beyond clusters: supramolecular networks self-assembled from nanosized silver clusters and inorganic anions. *Chem. – Eur. J.* **2016,** *22* (20), 6830-6836.

(38) Chen, Z.-Y.; Tam, D. Y. S.; Zhang, L. L.-M.; Mak, T. C. W. Silver thiolate nano-sized molecular clusters and their supramolecular covalent frameworks: an approach toward pre-templated synthesis. *Chem. – Asian J.* **2017,** *12* (20), 2763-2769.

(39) Huang, R.-W.; Dong, X.-Y.; Yan, B.-J.; Du, X.-S.; Wei, D.-H.; Zang, S.-Q.; Mak, T. C. W. Tandem silver cluster isomerism and mixed linkers to modulate the photoluminescence of cluster-assembled materials. *Angew. Chem. Int. Ed.* **2018,** *57* (28), 8560-8566.

(40) Wang, Q.-M.; Lin, Y.-M.; Liu, K.-G. Role of anions associated with the formation and properties of silver clusters. *Acc. Chem. Res.* **2015,** *48* (6), 1570-1579.

(41) Johnson, N. W., Convex polyhedra with regular faces. *Can. J. Math.* **1966,** *18*, 169-200.

(42) Bian, S.-D.; Wang, Q.-M. Snowman-like silver alkynyl cluster consolidated by templating chloride and peripheral trifluoroacetates. *Chem. Commun.* **2008,** (43), 5586-5588.

(43) Zhang, S.-S.; Su, H.-F.; Zhuang, G.-L.; Wang, X.-P.; Tung, C.-H.; Sun, D.; Zheng, L.-S. A hexadecanuclear silver alkynyl cluster based NbO framework with triple emissions from the visible to near-infrared II region. *Chem. Commun.* **2018,** *54* (84), 11905-11908.

(44) Spek, A. PLATON SQUEEZE: a tool for the calculation of the disordered solvent contribution to the calculated structure factors. *Acta Crystallogr. C* **2015,** *71* (1), 9-18.

(45) Sleigh, C.; Pijpers, A. P.; Jaspers, A.; Coussens, B.; Meier, R. J. On the determination of atomic charge via ESCA including application to organometallics. *J. Electron. Spectros. Relat. Phenomena.* **1996,** *77* (1), 41-57.

(46) Ward, R. L. A complete introduction to modern NMR spectroscopy (Macomber, Rodger S.). *J. Chem. Educ.* **1999,** *76* (4), 473.

(47) Li, G.; Lei, Z.; Wang, Q.-M. Luminescent molecular Ag–S nanocluster [Ag62S13(SBut)32](BF4)4. *J. Am. Chem. Soc.* **2010,** *132* (50), 17678-17679.

Table of Content